Supporting Information for Ab-initio force prediction for single molecule force spectroscopy made simple

Pooja Bhat, Wafa Maftuhin, Michael Walter

December 16, 2025

Contents

S1 Analytical expressions

S1.1 Differential equation in terms of the relative force f.

With the force given by $F = \alpha t$ at all times for a constant loading rate α and setting $k_r = 0$, we may replace t by F and write Eq. (4) in the main text as[1]

$$\frac{\partial P}{\partial F} = -\frac{k(F)}{\alpha} P(F) \, . \tag{S1}$$

Noting that $\alpha = F_{\max}/t_{\max}$ and using $f = F/F_{\max}$ we get

$$\frac{\partial P}{\partial f} = F_{\max} \frac{\partial P}{\partial F} = -t_{\max} k(f) P(f) \, . \tag{S2}$$

Using the definition of the relative rate $\kappa(f) = \tau k(f)$ with $\tau^{-1} = k(f = 0)$ leads to

$$\frac{\partial P}{\partial f} = -\frac{t_{\max}}{\tau} \kappa(f) P(f) \, . \tag{S3}$$

Note that

$$\int_0^\infty \frac{\partial P(f)}{\partial f} df = P(0) - P(\infty) = 1 \tag{S4}$$

holds independent of the form of $\kappa(f)$.

S1.2 Derivatives of $\partial P/\partial f$

The first derivative of the probability is given by Eq. (S3) and the second derivative is

$$\frac{\partial^2 P(f)}{\partial f^2} = \frac{t_{\max}}{\tau} \left[\frac{t_{\max}}{\tau} \kappa^2(f) - \frac{\partial \kappa(f)}{\partial f} \right] P(f) \, . \tag{S5}$$

The maximum of the distribution $\partial P/\partial f$ is found for the zeros of $\partial^2 P(f)/\partial f^2$, i.e. for

$$\frac{\partial \kappa(f)}{\partial f} = \frac{t_{\max}}{\tau} \kappa^2(f) \, . \tag{S6}$$

The third derivative reads

$$\frac{\partial^3 P(f)}{\partial f^3} = -\frac{t_{\max}}{\tau} \left[\frac{\partial^2 \kappa(f)}{\partial f^2} - \frac{3 t_{\max}}{\tau} \kappa(f) \frac{\partial \kappa(f)}{\partial f} + \left(\frac{t_{\max}}{\tau} \right)^2 \kappa^3(f) \right] P(f) \tag{S7}$$

and zeros of $\partial^3 P(f)/\partial f^3$ occurring for

$$\frac{\partial^2 \kappa(f)}{\partial f^2} - \frac{3t_{\max}}{\tau}\kappa(f)\frac{\partial \kappa(f)}{\partial f} + \left(\frac{t_{\max}}{\tau}\right)^2 \kappa^3(f) \ = 0 \tag{S8}$$

may be used to estimate the width of the distribution $\partial P(f)/\partial f$.

S1.3 Most probable force for the quadratic barrier

The expression for quadratic force dependent barrier is given by[1, 2]

$$\Delta H^{\ddagger}(f) = \Delta U^{\ddagger}(1-f)^2 \ , \tag{S9}$$

such that the corresponding relative rate is

$$\kappa_{\text{quadratic}}(f) = \exp(\beta \Delta U^{\ddagger} f(2-f)) \ . \tag{S10}$$

The most probable force is obtained by solving Eq. (S6), which can be written using $\kappa_{\text{quadratic}}(f^*)$ as[1]

$$2\beta \Delta U^{\ddagger}(1-f^*) = \frac{t_{\max}}{\tau}\kappa_{\text{quadratic}}(f^*) \ . \tag{S11}$$

Using $f^* = 1 - G$, we may write

$$G = \frac{t_{\max}}{\tau}\frac{1}{2\beta\Delta U^{\ddagger}} \exp\left[\beta \Delta U^{\ddagger}(1-G^2)\right] \ . \tag{S12}$$

With the shorthand

$$B = \frac{t_{\max}}{\tau}\frac{1}{2\beta\Delta U^{\ddagger}} \exp(\beta \Delta U^{\ddagger}) \tag{S13}$$

we arrive at

$$G = B \exp\left[-\beta \Delta U^{\ddagger} G^2\right] \ . \tag{S14}$$

Squaring Eq. (S14) and introducing $Q = 2\beta U^{\ddagger} G^2$ leads to

$$Q \exp(Q) = 2\beta \Delta U^{\ddagger} B^2 \ . \tag{S15}$$

This equation is solved by the Lambert W function represented by W, such that

$$Q = W(2\beta \Delta U^{\ddagger} B^2) \ . \tag{S16}$$

Upon substituting for Q and B we get

$$G^2 = \frac{1}{2\beta\Delta U^{\ddagger}} W\left(2\beta \Delta U^{\ddagger}\left[\frac{t_{\max}}{\tau}\frac{1}{2\beta\Delta U^{\ddagger}}\exp(\beta \Delta U^{\ddagger})\right]^2\right) \tag{S17}$$

and the most probable force is

$$f^* = 1 - G = 1 - \sqrt{\frac{1}{2\beta\Delta U^{\ddagger}} W\left(\frac{t_{\max}^2}{\tau^2}\frac{\exp(2\beta \Delta U^{\ddagger})}{2\beta\Delta U^{\ddagger}}\right)} \tag{S18}$$

Eq. (11) in the main text, i.e.

$$f^* = 1 - \sqrt{\frac{1}{2\beta\Delta U^\ddagger} W\left(\frac{t_{\max}^2}{2\beta\Delta U^\ddagger\, h^2\beta^2}\right)}\,, \tag{S19}$$

is obtained by expressing the theoretical life time of the bond in the Eyring form as $\tau = \beta h \exp(\beta\Delta U^\ddagger)$.

S1.3.1 Negative values for most probable force

The derived analytical expression for most probable force (Eq. (S19)) may produce negative values when the square root term turns greater than unity. In other sense, when the peak of $\frac{\partial P}{\partial f}$ seize to exist, as explained in the main text. The condition is given by,

$$\frac{1}{2\beta\Delta U^\ddagger} W\left(\frac{t_{\max}^2}{2\beta\Delta U^\ddagger\, h^2\beta^2}\right) > 1 \tag{S20}$$

or

$$W\left(\frac{t_{\max}^2}{2\beta\Delta U^\ddagger\, h^2\beta^2}\right) > 2\beta\Delta U^\ddagger \tag{S21}$$

Substituting for τ in the above equation,

$$W\left(\frac{t_{\max}^2}{\tau^2}\frac{\exp(2\beta\Delta U^\ddagger)}{2\beta\Delta U^\ddagger}\right) > 2\beta\Delta U^\ddagger \tag{S22}$$

From Lambert W function, $W(a) = Y$ implies $a = Y\exp(Y)$, and thus we have

$$\frac{t_{\max}^2}{\tau^2}\frac{\exp(2\beta\Delta U^\ddagger)}{2\beta\Delta U^\ddagger} > 2\beta\Delta U^\ddagger \exp(2\beta\Delta U^\ddagger) \tag{S23}$$

Simplifying the above equation results in

$$\frac{t_{max}}{\tau} > 2\beta\Delta U^\ddagger \tag{S24}$$

S1.4 Comparison to most probable force estimates from the literature

We will now compare different expressions from the literature where we express the terms appearing in our basic variables that are the barrier at zero force $\Delta U^\ddagger$ and the resulting theoretical lifetime of the bond $\tau = \beta h \exp(\beta\Delta U^\ddagger)$, the maximal force the bond can withstand $F_{\max}$ and the loading rate α.

S1.4.1 The Bell Evans model

The force dependent barrier for the Bell approximation can be expressed as

$$\Delta H^\ddagger(F) = \Delta U^\ddagger - F x^\ddagger\,, \tag{S25}$$

leading to the forward reaction rate [3]

$$k_f(t) = k_0 \exp[\beta F(t) x^\ddagger] \tag{S26}$$

or by making the connections $x^\ddagger = 2\Delta U^\ddagger / F_{\max}$ and $\tau = 1/k_0$ we arrive at

$$k_f(t) = \frac{1}{\tau} \exp[2\beta \Delta U^\ddagger f(t)] \, . \tag{S27}$$

This leads to the most probable force by Evans and Ritchie [4, 5]

$$F^* = \frac{k_B T}{x^\ddagger} \log\left(\frac{\alpha \tau x^\ddagger}{k_B T}\right) \tag{S28}$$

or

$$F^* = \frac{F_{\max}}{2\beta \Delta U^\ddagger} \log\left(\frac{\alpha \tau 2\beta \Delta U^\ddagger}{F_{\max}}\right) \, . \tag{S29}$$

Using $\alpha / F_{\max} = 1/t_{\max}$, the relative expression can be written as [2]

$$f^* = \frac{1}{2\beta \Delta U^\ddagger} \log\left(2\beta \Delta U^\ddagger \frac{\tau}{t_{\max}}\right) \, . \tag{S30}$$

The width of the distribution $\partial P(f)/\partial f$ can be obtained by solving Eq. (S8) leading to

$$\Delta f^* = \frac{1}{2\beta \Delta U^\ddagger} \log\left(\frac{3+\sqrt{5}}{3-\sqrt{5}}\right) = \frac{1.925}{2\beta \Delta U^\ddagger} \, . \tag{S31}$$

S1.4.2 Garg's general expression

Garg reported a very general expression for escape fields characterised by rates of the form[6]

$$k(f) = A(1-f)^{a+b-1} \exp\left(-B(1-f)^b\right) \, . \tag{S32}$$

Restricting to the quadratic barrier Eq. (S9) and expressing rates in the Eyring form leads to $A = 1/(\beta h), b = 2, a = -1$ and $B = \beta \Delta U^\ddagger$. The most probable relative force $\langle f \rangle = f^*$ for small α is asymptotically[6]

$$f^* = 1 - \sqrt{\frac{\log X}{\beta \Delta U^\ddagger}} \left[1 + \frac{1}{2 \log X} \left[-\frac{1}{2} \log\log X + \gamma\right] + \dots\right] \, . \tag{S33}$$

with $X = t_{\max}/(2\beta h \sqrt{\beta \Delta U^\ddagger})$ and $\gamma \approx 0.5772$ is the Euler-Mascheroni constant. Notably, also an asymptotic expression for the variance was derived.

S1.4.3 The Dudko-Hummer-Szabo model

Dudko and co-workers[7, 8] generally discuss two potentials, where the cusp-like potential characterised by $\nu = 1/b = 1/2$ leads to the force dependent

barrier expression of Eq. (S9). The authors furthermore set $a = 0$ such that rate expression Eq. (S32) becomes

$$k(f) = \frac{1}{\tau}(1-f)\exp(\beta(\Delta U^{\ddagger} - \Delta H^{\ddagger}))\,. \tag{S34}$$

Using the quadratic (cusp-like) barrier, the most probable force is given as[8]

$$f^* = 1 - \sqrt{\frac{1}{\beta \Delta U^{\ddagger}} \log\left(\frac{t_{\max}}{\tau}\frac{\exp(\beta\Delta U^{\ddagger}+\gamma)}{2\beta\Delta U^{\ddagger}}\right)} \tag{S35}$$

The authors also give the corresponding variance of the distribution, which is expressed in terms of our variables

$$\sigma_f^2 \approx \frac{\pi^2}{6(2\beta\Delta U^{\ddagger})^2}\left[\frac{1}{\beta\Delta U^{\ddagger}}\log\left(\frac{t_{\max}}{\tau}\frac{\exp(\beta\Delta U^{\ddagger}+1.064)}{2\beta\Delta U^{\ddagger}}\right)\right]^{-1}\,. \tag{S36}$$

Substituting for $\tau = \beta h \exp(\beta\Delta U^{\ddagger})$, the expression simplifies to,

$$\sigma_f^2 \approx \frac{\pi^2}{6(2\beta\Delta U^{\ddagger})^2}\left[\frac{1}{\beta\Delta U^{\ddagger}}\log\left(\frac{t_{\max}}{\beta h}\frac{\exp(1.064)}{2\beta\Delta U^{\ddagger}}\right)\right]^{-1}\,. \tag{S37}$$

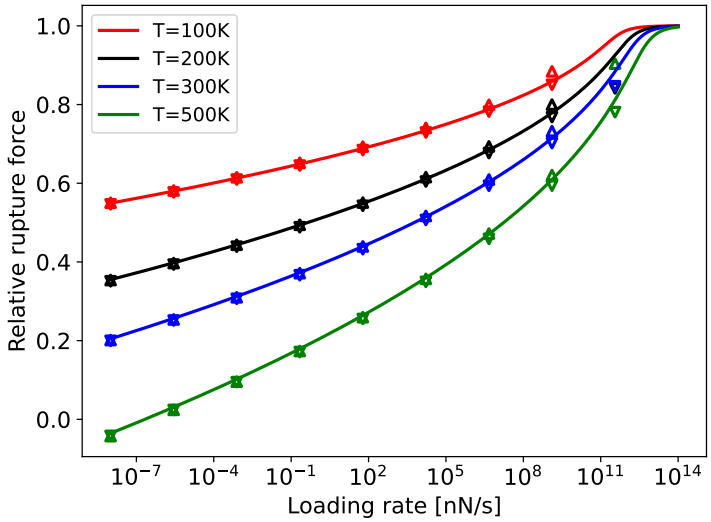

Figure S1: Most probable forces predicted for $AuAg_2$ from the forms by Garg [Eq. (S33) (down triangles)], Dudko et al. [Eq. (S35) (up triangles)] and our approach [Eq. (S19) (lines)].

Fig. S1 compares the predicted most probable forces from Garg [Eq. (S33)] and Dudko et al. [Eq. (S35)] with our quadratic expression [Eq. (S19)] considering the example of $AuAg_2$ in the main text ($F_{\max} = 2.38$ nN, $\Delta U^{\ddagger} = 1.8$ eV). All

three expressions closely match for the wide range of loading rates considered. All models have limitation of predicting negative most probable force values for very small loading rates (very slow pulling) and very high temperatures.

There is a difference in the limit of very large loading rates (very fast pulling). Then $t_{\max}$ gets small and the argument in the logarithms of Eqs. (S33) and (S35) may get smaller than unity. This leads to the square-root of negative values, i.e. to complex numbers. This limitation was already noted before[8]. The Lambert W function is positive also for arguments smaller than 1 and does not show this problem.

S1.4.4 The Friddle-De Yoreo model

Friddle et al [9] have considered both forward and backward reactions in their model. The forward rate is given by

$$k_f(F) = k_0 \exp\left(\beta\left[Fx^\ddagger - \frac{1}{2}k_c x^{\ddagger 2}\right]\right) \tag{S38}$$

where k_c (nN/Å) is the cantilever spring constant. We are considering experiments of long polymer chains, such that k_c (nN/Å) is much smaller than the spring constant of the potential, i.e. the limit $k_c \to 0$. In this case, the forward rate coincides with the Bell rate. The backward rate is given by

$$k_r(F) = k_f(F) \exp\left(\beta\left(\Delta U^\ddagger - \frac{F^2}{2k_c}\right)\right) \tag{S39}$$

which is strongly suppressed for $k_c \to 0$, except for extremely small F. The backward rate can therefore be ignored in the force regime of interest in the main text. The model therefore coincides with the Bell model for the force range of interest here. It should be better suited for very small forces where the back-reaction can not be ignored, however.

The mean rupture force then is concluded by the expression,

$$F^* = F_{eq} + F^\ddagger \log\left(1 + \frac{\alpha \exp(-\gamma)}{k_0(F_{eq})F^\ddagger}\right) \tag{S40}$$

where $F_{eq} = \sqrt{2k_c\Delta U^\ddagger}$ and $F^\ddagger = 1/\beta x^\ddagger$. Considering there is no backward reaction, we have the equilibrium force at $F_{eq} = 0$. Identifying $F^\ddagger = F_{\max}/(2\beta\Delta U^\ddagger)$, the mean rupture force reduces to

$$F^* = \frac{F_{\max}}{2\beta\Delta U^\ddagger} \log\left(1 + \frac{2\beta\Delta U^\ddagger \alpha \exp(-\gamma)}{k_0(0)F_{\max}}\right) \tag{S41}$$

where $k_0(0)$ corresponds to the rate at zero force which corresponds to the lifetime of the bond, i.e. $1/k_0(0) = \tau$. The relative most probable force is

$$f^* = \frac{1}{2\beta\Delta U^\ddagger} \log\left(1 + \frac{2\beta\Delta U^\ddagger \tau \exp(-\gamma)}{t_{\max}}\right) . \tag{S42}$$

The paper [9] also discusses two primary regimes based on the loading rate values: a linear regime in the slow loading limit $\langle F(\alpha)\rangle^*_{\alpha\to 0} = F_{eq}+\alpha/k_0(F_{eq})$ and a nonlinear regime in the fast loading limit, $\langle F(\alpha)\rangle^*_{\alpha\to\infty} = F^\ddagger \log(\exp(-\gamma)\alpha\tau/F^\ddagger)$. This gives rise to a relative expression in the fast loading limit very similar to Bell expression Eq. (S30) given by,

$$\langle f(\alpha)\rangle^*_{\alpha\to\infty} = \frac{1}{2\beta\Delta U^\ddagger}\log\left(\frac{2\beta\Delta U^\ddagger\tau\exp(-\gamma)}{t_{\max}}\right) \tag{S43}$$

This implies the mean rupture force is linear in nature and that the Friddle model is applicable where force is acting linearly on the molecule. Notably the equilibrium force expression for N bond break uses Lambert W function [9] and is independent of the cantilever spring constant k_c.

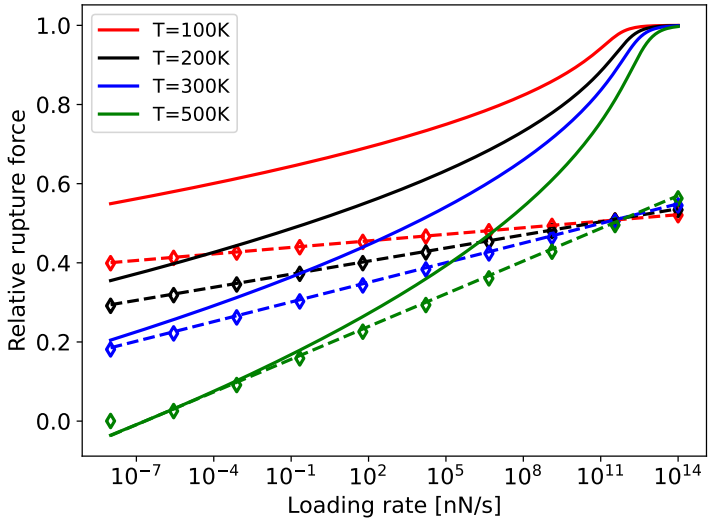

Figure S2: Most probable force calculated for $AuAg_2$ from the forms by Friddle [Eq. (S42) (open symbols)], Bell [Eq. (S30) (broken lines)] and our approach [Eq. (S19) (lines)]

From Fig. S2, we see that the Friddle expression in the case of single rupture event without rebinding [Eq. (S42)] closely relates to the Bell expression [Eq. (S30)]. We see our expression Eq. (S19) deviates at higher loading rates due to its quadratic form. At lower loading regime, the Friddle expression goes to zero (since $F_{eq} = 0$) but the Bell and our quadratic form gives out negative values.

S1.4.5 The Friddle unified model

In an earlier paper by Friddle alone [10], the mean escape force for the complete force spectrum was established for thermally activated barrier. The model de-

scribes a way to use it at lower loading rates where Bell, Garg, Dudko and our model end up with negative values. The mean force is given by,

$$f^* = 1 - \sqrt{1 - \frac{1}{\beta \Delta U^{\ddagger}} \log\left(1 + \frac{2\beta \Delta U^{\ddagger} \tau \exp(-\gamma)}{t_{max}}\right)} \tag{S44}$$

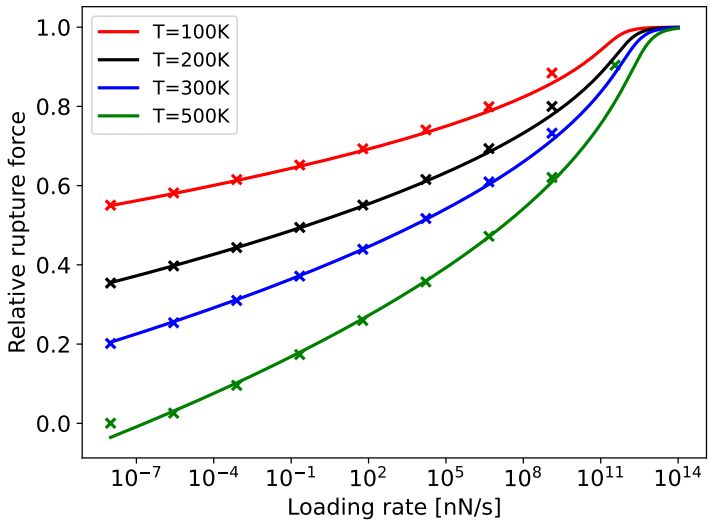

Figure S3: Most probable force calculated for $AuAg_2$ from the forms by unified model expression by Friddle [Eq. (S44)(symbol x)] and our approach [Eq. (S19) (lines)]

From the Fig. S3, we see that the values from unified model by Friddle resembles our quadratic model for large range of loading rates. However when the relative rupture force reach unity, it encounters the problem of values going complex. The corresponding variance expression expressed in terms of our variables is given by,

$$\sigma_f^2 \approx \left[\frac{1}{2\beta \Delta U^{\ddagger}\left(1 + \frac{t_{max}}{2\beta \Delta U^{\ddagger} \tau}\right)}\right]^2 \left[1 - \frac{1}{\beta \Delta U^{\ddagger}} \log\left(1 + \frac{t_{max} \exp(-\gamma)}{2\beta \Delta U^{\ddagger} \tau}\right)\right]^{-1} \tag{S45}$$

S1.4.6 The Bullerjahn model

The Bullerjahn model [11] has an analytical expression of the rupture force distribution over an entire range of loading rates. This model is applicable even at forces higher than the maximum force, i.e. in the ballistic regime. It makes

use of a cusp-like potential defined by an absorbing boundary and accounts for both drift and diffusion parameters. The model parameters (diffusion coefficient, energy barrier and distance to transition state) are obtained by global fitting of experimental data at various loading rates using systematic Bayesian (i.e. updating the probabilities of parameters as and when new data is available) analysis. This helps in efficient analysis of experimental unbinding data. This model is applicable across a wide range of loading rates, with the exception of a narrow range near the critical loading rate. Additionally, in the limit of the low loading range, the model reduces to Dudko-Hummer Szabo model for cusp-like potential which closely relates to our Quadratic Barrier model.

S1.4.7 Other models

Several other models account for specific issues of single molecule force spectroscopy force measurements. For example, the model by Maitra and Arya [12] accounts for device stiffness in force measurements and considers a linear-cubic potential explicitly. In addition, a popular model by Hummer and Szabo [13] considers a stochastic model to extract kinetic information (3 adjustable parameters) from pulling experiments which the phenomenological Bell model fails to consider. This step is believed to be important in the experimentally relevant regime.

S1.5 Quadratic force width

We have relative quadratic barrier rate and the derivatives given by,

$$\kappa(f) = \exp(\beta \Delta U^{\ddagger} f(2-f)) \tag{S46}$$

$$\frac{\partial \kappa(f)}{\partial f} = 2\beta \Delta U^{\ddagger}(1-f)\kappa(f) \tag{S47}$$

$$\frac{\partial^2 \kappa(f)}{\partial f^2} = 2\beta \Delta U^{\ddagger}\kappa(f)(2\beta \Delta U^{\ddagger}(1-f)^2 - 1) \tag{S48}$$

The above equations are required in analytically estimating the width of the $\partial P(f)/\partial f$ given by Eq. (S8) which simplifies to

$$0 = 2\beta \Delta U^{\ddagger}(2\beta \Delta U^{\ddagger}(1-f)^2 - 1) - \frac{3t_{\max}}{\tau} 2\beta \Delta U^{\ddagger}(1-f)\kappa(f) + \left(\frac{t_{\max}}{\tau}\right)^2 \kappa^2(f) \tag{S49}$$

Rearranging the above equation,

$$2\beta \Delta U^{\ddagger}(2\beta \Delta U^{\ddagger}(1-f)^2 - 1) = \kappa(f)\frac{t_{\max}}{\tau}\left(6\beta \Delta U^{\ddagger}(1-f) - \kappa(f)\frac{t_{\max}}{\tau}\right) \tag{S50}$$

Let $2\beta \Delta U^{\ddagger}(1-f) = R$, then

$$2\beta \Delta U^{\ddagger}(R(1-f) - 1) = \kappa(f)\frac{t_{\max}}{\tau}\left(3R - \kappa(f)\frac{t_{\max}}{\tau}\right) \tag{S51}$$

or

$$R^2 - 2\beta\Delta U^{\ddagger} = \kappa(f)\frac{t_{\max}}{\tau}\left(3R - \kappa(f)\frac{t_{\max}}{\tau}\right) \tag{S52}$$

or

$$R^2 - 3\frac{\kappa(f)t_{\max}}{\tau}R + \left(\left(\frac{\kappa(f)t_{\max}}{\tau}\right)^2 - 2\beta\Delta U^{\ddagger}\right) = 0 \tag{S53}$$

Solving the above quadratic equation simplifies to,

$$R = \frac{1}{2}\left(\frac{3\kappa(f)t_{\max}}{\tau} \pm \frac{\kappa(f)t_{\max}}{\tau}\sqrt{5 + \frac{8\beta\Delta U^{\ddagger}\tau^2}{(\kappa(f)t_{\max})^2}}\right) \tag{S54}$$

Also, $\frac{\tau}{\kappa(f)} = \exp(\beta\Delta U^{\ddagger}(1-f)^2)/A$ where $A = 1/\beta h$ is exponential prefactor. Let $f = 1 - G$, substituting for R and $\kappa(f)$ gives,

$$4\beta\Delta U^{\ddagger}G\exp(-\beta\Delta U^{\ddagger}(1-G^2)) = \frac{t_{\max}}{\tau}\left(3 \pm \sqrt{5 + \frac{8\beta\Delta U^{\ddagger}\exp(2\beta\Delta U^{\ddagger}G^2)}{(At_{\max})^2}}\right) \tag{S55}$$

The term $\frac{8\beta\Delta U^{\ddagger}\exp(2\beta\Delta U^{\ddagger}G^2)}{(At_{\max})^2}$ interestingly has an energy ratio parameter $\beta\Delta U^{\ddagger}$ in the numerator and a time ratio parameter At_{max} in the denominator. Let us name it as M and analyze its contribution with variation in temperature and loading rate values.

$$M = \frac{8\beta\Delta U^{\ddagger}\exp(2\beta\Delta U^{\ddagger}G^2)}{(At_{\max})^2} \tag{S56}$$

For strong bonds as in our case, the dissociation energy $\Delta U^{\ddagger} \gg k_B T = 1/\beta$. Generally, the dissociation energy is greater than 1 eV. Let $\Delta U^{\ddagger} > 1.05$ eV, then the energy ratio $\beta\Delta U^{\ddagger}$ is approximately about 240 for $T = 50$ K and about 12 for $T = 1000$ K. The denominator term A^2 imply that even larger variation in temperatures do not affect the overall value ($A^2 = (k_B T/h)^2$). Here k_B is the Boltzmann constant and h is Planck's constant.
For analyzing the effect of loading rate, we consider two extreme cases of relative force values.

1. When $f \to 1$ i.e. at very high loading rates or shorter t_{max}, $\exp(2\beta\Delta U^{\ddagger}G^2) = \exp(2\beta\Delta U^{\ddagger}(1-f)^2) \approx 1$. The denominator $(At_{\max})^2$ has contribution mainly from exponential prefactor A squared, which contributes more than $1\text{x}10^{24}$ for temperatures greater than 50 K. Thus the contribution of M on the whole is negligible.

2. At smaller loading rates when $f \to 0$, $\exp(2\beta\Delta U^{\ddagger}G^2) \approx \exp(2\beta\Delta U^{\ddagger}) \approx (\tau A)^2$. Then $M \approx \frac{8\beta\Delta U^{\ddagger}\tau^2}{(t_{max})^2}$. However at these smaller forces we have very high t_{max} values and thus the denominator contribution will be larger than the numerator. Hence the contribution of M is again negligible.

Thus the exponential term value ranges between $(\tau A)^2 > \exp(2\beta\Delta U^\ddagger G^2) > 1$ for $0 < f < 1$. However, for a given exponential value, we have corresponding high denominator contribution (either $(t_{max})^2$ in lower force region or A^2 in higher force region) to nullify the effect of high exponential values or to reduce the overall contribution of M. Thus for all loading rates and temperatures,

$$M = \frac{8\beta\Delta U^\ddagger \exp(2\beta\Delta U^\ddagger G^2)}{(At_{\max})^2} << 5 \tag{S57}$$

and further simplifying the equation we will have,

$$4\beta\Delta U^\ddagger G = \frac{t_{\max}}{\tau}\left(3 \pm \sqrt{5}\right)\exp(\beta\Delta U^\ddagger)\exp(-\beta\Delta U^\ddagger G^2) \tag{S58}$$

Let $B = \frac{t_{\max}}{\tau}\frac{\exp(\beta\Delta U^\ddagger)}{4\beta\Delta U^\ddagger}\left(3 \pm \sqrt{5}\right)$, then $G = B\exp(-\beta\Delta U^\ddagger G^2)$ and we have,

$$2\beta\Delta U^\ddagger G^2 = 2\beta\Delta U^\ddagger B^2 \exp(-2\beta\Delta U^\ddagger G^2) \tag{S59}$$

Now consider $Q = 2\beta\Delta U^\ddagger G^2$, then

$$Q\exp(Q) = 2\beta\Delta U^\ddagger B^2 \tag{S60}$$

or $Q = W(2\beta\Delta U^\ddagger B^2)$ where $W(x)$ is the Lambert W function. Substituting for B and Q, we get,

$$G^2 = \frac{1}{2\beta\Delta U^\ddagger} W\left(\frac{t_{\max}^2 A^2}{8\beta\Delta U^\ddagger}\left(3 \pm \sqrt{5}\right)^2\right) \tag{S61}$$

or in terms of relative most probable force $f^* = 1 - G$, as the roots correspond to the rupture force error on either side of the distribution,

$$f^* = 1 - \sqrt{\frac{1}{2\beta\Delta U^\ddagger} W\left(\frac{t_{\max}^2 A^2}{8\beta\Delta U^\ddagger}\left(3 \pm \sqrt{5}\right)^2\right)} \tag{S62}$$

The width of the distribution is the difference between the roots given by,

$$\Delta f^* = \sqrt{\frac{1}{2\beta\Delta U^\ddagger}}\left(\sqrt{W\left(c\,(a+b)^2\right)} - \sqrt{W\left(c\,(a-b)^2\right)}\right) \tag{S63}$$

where $a = 3$, $b = \sqrt{5}$ and $c = \frac{t_{\max}^2 A^2}{8\beta\Delta U^\ddagger} = \frac{t_{\max}^2}{8\beta\Delta U^\ddagger h^2\beta^2}$ corresponding to the most probable quadratic force given by,

$$f^* = 1 - \sqrt{\frac{1}{2\beta\Delta U^\ddagger} W\left(\frac{t_{\max}^2}{2\beta\Delta U^\ddagger\, h^2\beta^2}\right)}\,, \tag{S64}$$

The quadratic width expression Eq. (S63) rightly predicts the increase in width of $\frac{\partial P}{\partial f}$ distribution with increase in loading rates and decrease in temperature as observed in Fig. 3 for probability distribution in the main text.

S1.6 Comparison to numerical and literature force widths expressions

S1.6.1 Numerical width

The width of a distribution can be numerically attributed to twice the standard deviation or analytically obtained by considering Full Width at Half Maximum of the distribution. For a distribution $f(x)$, the variance w.r.to x or the standard deviation squared can be numerically given by,

$$\sigma^2 = \langle (x-\mu)^2 \rangle = \int (x'-\mu)^2 f(x') dx' \tag{S65}$$

where $\mu = \int x' f(x) dx'$ is the mean x value. Thus for $\frac{\partial P(f)}{\partial f}$ distribution, the variance σ^2 can be numerically obtained as,

$$\sigma^2 = \langle (f-f^*)^2 \rangle = \int (f'-f^*)^2 \frac{\partial P(f')}{\partial f'} df' \tag{S66}$$

where $f^* = \int f' \frac{\partial P(f')}{\partial f'} df'$ is the mean rupture force of the distribution. The numerical width is then 2σ.

S1.6.2 Numerical width from derivatives of $\frac{\partial P(f)}{\partial f}$

Another way of obtaining numerical width is by setting $\frac{\partial^3 P(f)}{\partial f^3} = 0$, the difference between the roots then correspond to a different numerical width. The expression for analytical quadratic width is formulated using this approach [Eq. (S63)]. We can arrive at the values numerically, as well by calculating $\frac{\partial P(f)}{\partial f}$ and its derivatives numerically.

S1.6.3 The Bell width

Similar to expression for quadratic width, using Bell rate and their derivatives and using Eq. (S8) we can arrive at an expression for Bell width given by $\Delta f^* = 1.925/2\beta\Delta U^\ddagger$ i.e Eq. (S31). We see that the expression is independent of loading rate but is directly proportional to temperature.

S1.6.4 The Dudko width

Dudko and co-workers [7, 8] have their analytical variance expression given by Eq. (S37) for cusp-like potential, then the corresponding analytical width, $2\sigma_f$ is,

$$2\sigma_f \approx 2\sqrt{\frac{\pi^2}{6(2\beta\Delta U^\ddagger)^2}\left[\frac{1}{\beta\Delta U^\ddagger}\log\left(\frac{t_{\max}}{\beta h}\frac{\exp(1.064)}{2\beta\Delta U^\ddagger}\right)\right]^{-1}}. \tag{S67}$$

S1.6.5 The Friddle width

The analytical variance expression in unified model by Friddle [10] given by Eq. (S45). The corresponding width then is given by,

$$2\sigma_f \approx 2\sqrt{\left[\frac{1}{2\beta\Delta U^{\ddagger}\left(1+\frac{t_{max}}{2\beta\Delta U^{\ddagger}\tau}\right)}\right]^2\left[1-\frac{1}{\beta\Delta U^{\ddagger}}\log\left(1+\frac{t_{max}\exp(-\gamma)}{2\beta\Delta U^{\ddagger}\tau}\right)\right]^{-1}}. \tag{S68}$$

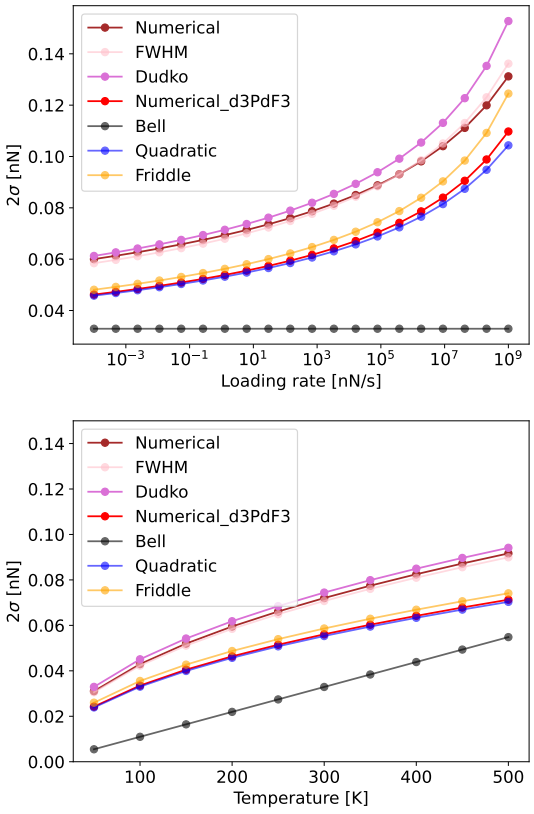

Figure S4: Width of the distribution calculated for $AuAg_2$ by numerical methods and using analytical expressions at different loading rates and temperatures.

Considering the width predictions for $AuAg_2$ molecule in Fig. S4, we see that the Bell widths are lower in comparison to other widths and is independent of loading rates as seen in Eq. (S31). However, the numerical widths (related to FWHM) closely relate to Dudko widths in the experimentally suitable loading rate range ($\approx$ 10 nN/s) and for all temperature ranges. Our quadratic width and Friddle width relate closely to numerical widths obtained after setting the

higher derivative of the probability distribution to zero. Hence, we have used the Dudko widths [Eq. (S67)] for analytical rupture force error calculations for all considered molecules.

S2 Influence of structure size

The experimental setup of SMFS involves a flexible cantilever attached to atomic force microscopy (AFM) tip. The polymer of interest is connected to the tip at one end while the other end attached to the surface. This method is suitable to study protein unfolding, stretching and finding interaction forces, in addition to determining rupture forces at single molecular level by using controlled forces on polymer of interest [14]. Under controlled environment, the polymer stretched beyond its elastic limit results in breaking of its weakest bond. This influences the position of cantilever whose deflection can be measured.

In such experiments, if the long molecule considered has ring structured moieties, the rupture forces totally depend on bond breaking in these structures [15]. For example, in cyclopropanes, the pulling causes strain in the ring area and breaks one of the carbon-carbon bonds in the ring. During this bond break, the force remains constant for a period of time while elongating the molecule. Since the breakage does not cause molecule fragmentation in these molecules, the further pull will result in force increase. This force extension curve plateau is the experimental rupture force and the slope corresponds to the total spring constant of the system (molecule+comonomers+cantilever).

S2.1 Cyclopropane ring opening

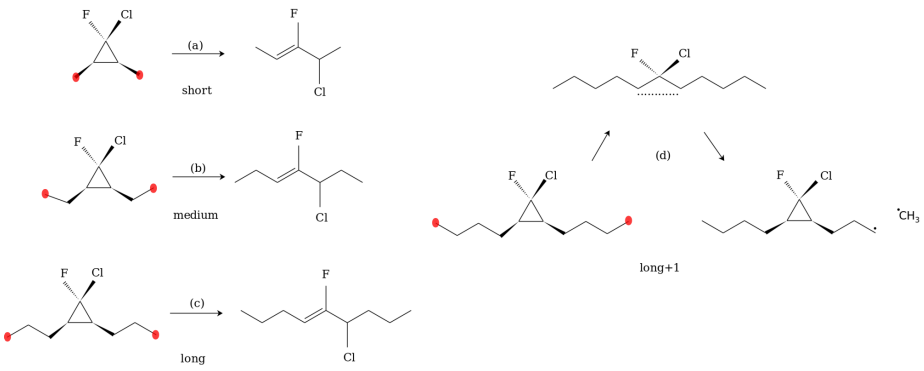

Figure S5: Schematic of initial and final product states by COGEF simulations for syn-Cl gCFC monomer of different lengths. The molecular pulling points are inicated by red symbols.

To understand the influence of monomer sizes on ring opening reaction, we have considered four cyclopropane molecules with increasing lengths namely short,

medium, long and long+1 monomers. COGEF simulations are carried out by pulling end carbon atoms by a step-size of 0.075 Å in each case. The molecule in each step is relaxed using ASE's FIRE algorithm and uses PBE functional of GPAW for calculating energies and forces. The product state after ring opening (or bond break) is visualized and shown in Fig. S5. Larger step-size might increase the forces rapidly which might skip the force required to open the cyclopropane ring and result in a different product state.

During pulling, one of the C-C bonds inside the ring breaks, opening the cyclopropane ring and the chlorine atom attached to carbon migrates. Here we see the movement is to the right of the central bond. However, in symmetric molecules, the migration of halogen to the left or right has a local minima and hence interconversion between them is possible [16]. The opposite side of movement gains a double bond to compensate for tetrahedral bonding of carbon.

In the case of long+1 monomer in Fig. S5 (d), we see that the pulling increases the bond length of the C-C in cyclopropane ring almost opening it, but further pulling eventually results in breaking of a bond in elastic region of the molecule and also result in ring reformation. In this case, migration of chlorine atom is not observed. This contrasting product state may be due to non-consideration of temperature effect in COGEF.

S2.2 Energy and forces acting on monomer while pulling

We are interested in computing the barrier for the ring opening of cyclopropane. Assuming the validity of the approximation of the quadratic force dependence of the barrier, we need to determine the maximum force corresponding to the ring opening as well as the energy needed in absence of force.

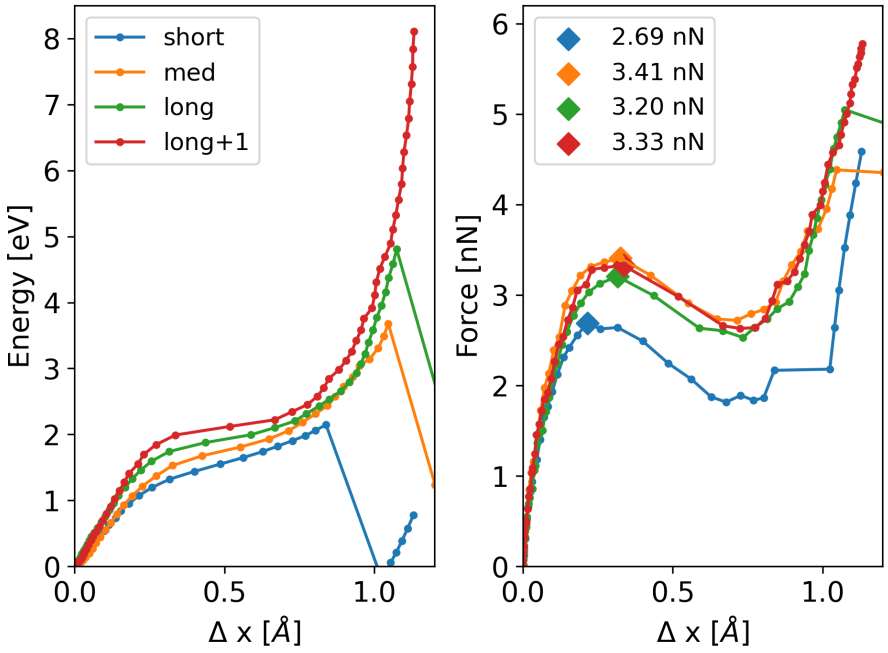

Figure S6: Energy and force curves for considered monomer sizes with respect to the length of the breaking bond (Δx)

The energy and forces for considered monomers is depicted in Fig. S6 plotted against increasing distance of most probable breaking C-C bond Δx. We see that the energy and forces vary significantly depending on the size of the monomer.

For the short monomer, the existence of only one carbon atom on either side of cyclopropane ring indicate there are no extra energy contributions (e.g. rotation, dihedral angles). On the other hand, the longer carbon chains in medium, long and long+1 monomers having extra carbon atoms can be attributed to increased energy and hence represent elastic part of the molecule. Therefore the exact barrier required for the ring opening has to be calculated by NEB method [17] or 3s-COGEF [18]. In this paper, we have used simple NEB approach and for this particular molecule, independent of the size, we obtain a barrier of around 2 eV for COGEF induced reactions.

Regarding the maximum force $F_{\max}$, we see that there is no notable change for medium, long and long+1 monomers, with the values of 3.21 nN, 3.41 nN and 3.33 nN respectively. Even with a completely different product state for long+1 monomer, the maximum force required for cyclopropane ring opening is similar to other monomers having elastic energy contributions. This suggests that the maximum force has no influence on elastic part of the molecule but only varies if the molecule is very rigid.

Hence, we have continued our studies with medium sized monomers for all

molecules owing to no major changes in barrier and $F_{\max}$ on further increasing the length of monomers.

S3 Available single molecule force spectroscopy experiments

Table S1: Loading rate calculations from force curves. The experimentally determined free energy of activation ($\Delta U^{\ddagger}$) is in eV and experimental measured forces (F_{mp}) are given in nN. Retraction velocity of the cantilever (v_c) is given in nm/s. The force constant (k) used in calculation of loading rate is in pN/Å, the values marked by $^{+}$ denotes cantilever spring constant. The loading rate (α) is in nN/s, and the asterisk * denote derived values.

Molecule	$\Delta U^{\ddagger}$	F_{mp}	v_c	k	α
syn-Cl-gCFC (CP1)	1.78, 1.95[19]	1.5 [19]	300	2^{+}	6^{*}
anti-Cl-gCFC (CP2)	1.6[19]	1.29 [19]	300	0.75	2.3^{*}
gDBC PNB (CP3)		0.74 [20]	3000		3.5^{a}
gDBC PB (CP4)	1.39 [21]	1.21 [20]	3000		3.5^{a}
gDCC PB/cis gDCC (CP5)	1.58 [20]	1.33 [20, 22]	3000		3.5^{a}
trans gDCC (CP6)	1.65 [23]	2.3 [22]	3000	2^{+}	6^{*}
gDCC PNB (CP7)		0.9 [20]	3000		3.5^{a}
E-α-alkene-gDCC (CP8)	1.33[24]	0.8 [24]	300	1.236	3.7^{*}
Z-α-alkene-gDCC (CP9)	1.33[24]	1.16 [24]	300	1.692	5.1^{*}
trans-BCB (BCB1)	1.99 [25]	1.5 [22]	300	2^{+}	6^{*}
cis-BCB (BCB2)	1.99 [25]	1.37[22]	300	2^{+}	6^{*}
Z-α-alkene-BCB (BCB3)	1.99 [25]	1.25 [25]	300	1.563	4.7^{*}
E-α-alkene-BCB (BCB4)	1.99 [25]	0.92 [25]	300	1.563	4.7^{*}

[a] The mean value of 3.5 nN/s for given loading rate of 2-5 nN/s in ref. [20]

Table S1 gives an overview of the experimental forces F_{mp}, cantilever velocities v_c, spring constants k and loading rates α. The method of obtaining spring constant values from fore-extension curve along with loading rate estimations are discussed in the following section.

S4 Estimation of the experimental loading rate

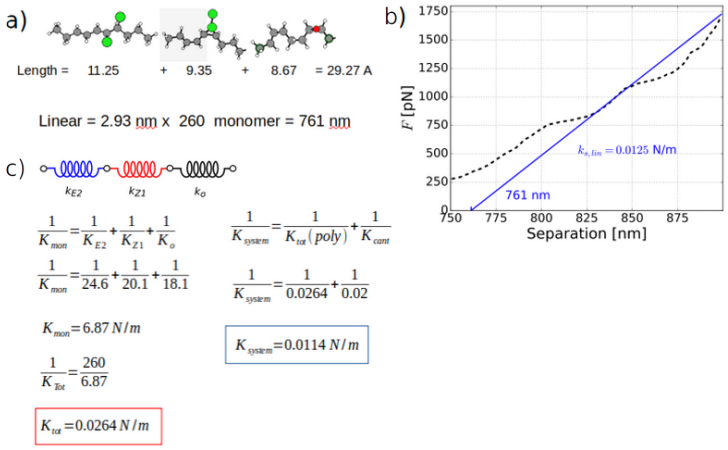

Figure S7: a) Single monomer from relaxed configurations with the total distance d and the number of monomers obtained from zero fit function unfolded polymer of 761 nm length from b) linear fit (blue line) from the experimental force extension curve [26]. c) Spring constant calculation of polymer (red square) and the total system including (blue square).

In SMFS experiments, the AFM cantilever in general moves at a constant velocity v_c. This velocity is related to the loading rate α through the force constant k which contains elastic responses from the polymer as well as from the cantilever as $\alpha = kv_c$. One way to obtain this spring constant is by considering spring constant values of individual monomers constituting the polymer and then calculating the net k_{system} for the whole polymer used in the experimental setup as shown in Fig. S7 c).

Another way to extract the spring constant value is from the slope of experimental force curve (see Fig. S7 b). The plateau in the force extension curve discloses the bond break event in the considered monomer. At this force, the polymer extends upto a certain length before the further increase in forces. The spring constant of curve after the plateau represents the total spring constant of the polymer (i.e., monomers + comonomers + cantilever). In this paper, we have used this measured spring constant to obtain an estimate of experimental loading rate.

However, in cases where the measured value was higher (in principle not possible) than the cantilever spring constant, the latter was used for loading rate estimation. The reason for higher measured value may be due to fitting errors or due to the domination of cantilever spring constant on the force curve. The values of considered spring constant and obtained loading rate values are listed in Table S1.

S5 Computed barriers, maximal forces, most probable force

The dissociation energy barrier correspond to the force independent thermal barrier for ring opening reactions. Considering initial and final states from COGEF after removal of force constraints gives us a thermal barrier. However, for ring structured molecules, Woodward Hoffmann/Woodward-Hoffmann-DePuy (WH/WHD) rules dictate the thermal ring opening reactions. Therefore, it is important to make sure that the COGEF ring opening reaction is not in violation with these rules.

S5.1 Woodward-Hoffmann/Woodward-Hoffmann DePuy rules

The WH rule[27, 28] based on orbital symmetry states that cyclopropanes undergo 'disrotatory' and benzocyclobutenes undergo 'conrotatory' motion during thermal ring opening reactions. Disrotatory implies constituents attached to breaking bond move in opposite directions [both inwards or both outwards]. Conrotatory implies constituents attached to the breaking bond both move in same direction [both right or both left].

Further, the disrotatory direction of rotation in cyclopropanes, 'inward' or 'outward' is decided based on WHD rule[29]. This decision is based on the migration of cis or trans positioned halogen atom with respect to the ring. The rotation can be visualized for simulated reactions or can be evaluated by calculating the rotating angles[30].

If the COGEF ring opening reaction violates the rule, the rule adhering final state is obtained by rotating constituents along one side of the broken bond in opposite direction.

Experimentally, it is observed that the molecules CP1, CP6, BCB2, BCB4 violate the thermal ring opening rules. The COGEF simulations for CP1, BCB2, BCB4 also realizes WH-forbidden product states. Thus, for these molecules, we have calculated the barriers for forbidden as well as allowed reaction. The schematics and NEB paths of reactions are shown in Table S3.

However, for the trans gDCC (CP6) molecule disagreeing with WH rules [25], studied in detail by Wollenhaupt group [31, 16], the desired product state from COGEF is not realized. It can be seen that a different bond breaks upon mechanophore extension. Therefore, for the calculation of $\Delta U^{\ddagger}$ using NEB, the possible WH allowed product state configuration in the thermal limit (2,3-dichloroalkene) is forced. The reaction from COGEF and thermal reaction can be referred from Table S3.

S5.2 COGEF $F_{\max}$ consideration

COGEF calculations may not always produce experimental migration of halide [32] reactions after ring opening in molecules. As in the case of trans gDCC (CP6), central C-C bond breaks but further increase in length does not help the migration of halide to produce 2,3-dichloroalkene state. Instead a different C-C

bond breaks and diradical species at the centre is maintained. For such cases, we have used the $F_{\max}$ value calculated from the COGEF, as the ring opening with bond break is still observed, which decides the $F_{\max}$ as observed in Fig. S6 for long+1 monomer. Hence, maximum force from COGEF is highly beneficial parameter for force induced reactions.

S5.3 COGEF $F_{\max}$ value discrepancy

Usage of different exchange-correlation functional for simulations can also impact the molecular system parameters. As shown in the Table S2, discrepancy exists for $F_{\max}$ values calculated using B3LYP/6-31G* [33] functional by Klein et al. and the PBE [34] functional by us. It is well known from the literature that the $F_{\max}$ values predicted from the hybrid functionals such as B3LYP are higher than pure GGA functional such as PBE [35]. Despite the differences, the $F_{\max}$ follow similar trend in related molecules (Ex: cis and trans gDCC). We have considered $F_{\max}$ values from PBE functional throughout the paper.

Table S2: COGEF $F_{\max}$ and barriers $\Delta U^{\ddagger}$ from NEB calculations for considered ring structured molecules. The values in the brackets indicate barriers for anti-WH/WHD reaction. The COGEF maximum forces, $F^*_{\max}$ (B3LYP/6-31G*) from ref. [32] are also listed. $F_{\max}$, $F^*_{\max}$ are in nN, $\Delta U^{\ddagger}$ is in eV.

Molecule	$\Delta U^{\ddagger}$	$F_{\max}$	$F^*_{\max}$ [32]
syn-Cl-gCFC (CP1)	1.84 (1.97)	3.4	3.5
anti-Cl-gCFC (CP2)	1.60	3.36	3.2
gDBC PNB (CP3)	1.32	3.04	3.3
gDBC PB (CP4)	1.50	3.39	3.7
gDCC PB/cis gDCC (CP5)	1.70	3.58	3.8
trans gDCC (CP6)	1.82	4.74	5.2
gDCC PNB (CP7)	1.55	3.27	3.4
E-α-alkene-gDCC (CP8)	1.27	2.81	3.2
Z-α-alkene-gDCC (CP9)	1.32	3.41	3.7
trans-BCB (BCB1)	1.48	3.87	4.1
cis-BCB (BCB2)	1.64 (2.12)	3.4	3.7
Z-α-alkene-BCB (BCB3)	1.2	3.45	3.7
E-α-alkene-BCB (BCB4)	1.16 (1.85)	2.86	3.1

S5.4 Most probable force from COGEF product state

If one has to neglect the rotation rules and consider COGEF product state directly for calculation of force independent ring opening barriers, R^2 value for most probable forces comes up to 0.68 against 0.81 after applying WH/WHD rule corrections. The rupture forces calculated by considering NEB barriers from COGEF product states alone is given in Fig. S8.

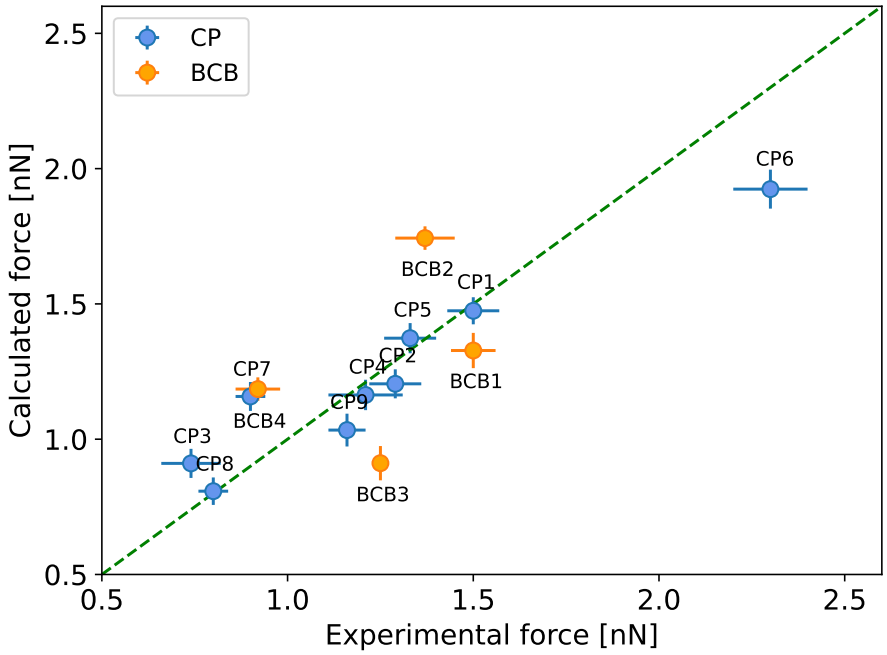

Figure S8: Comparison of predicted most probable forces with experimental results without WH/WHD corrections

S5.5 Comparison of maximum forces and most probable forces

Here we use $F_{\max}$ from COGEF and barriers according to Woodward-Hoffmann rules to determine the most probable forces. Diarylethene (DAE) mechanophores from a recent study[36] is also included. More details can be found in the main text. We compare $F_{\max}$ and our most probable force predictions to the measured rupture forces[26, 20, 21, 25, 24, 22, 36].

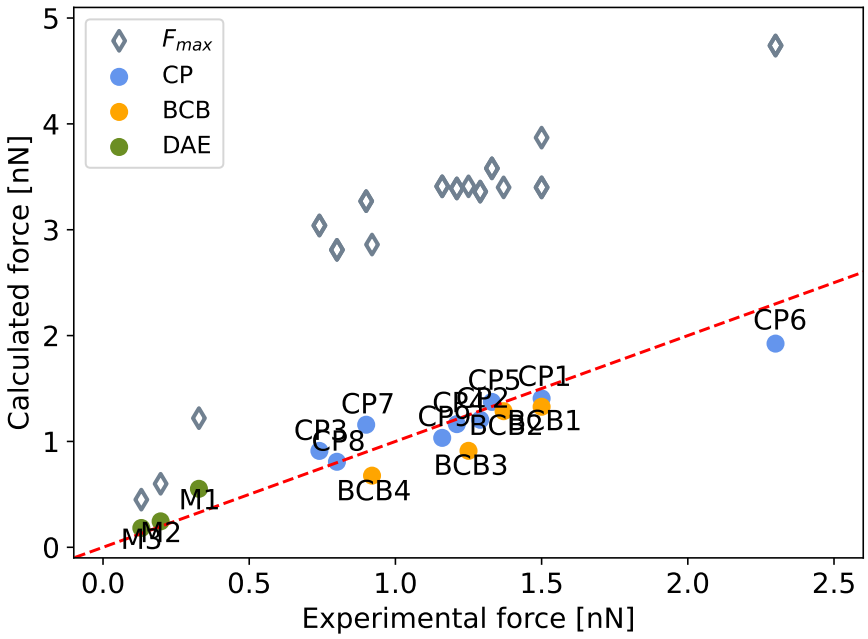

Figure S9: Comparison of $F_{\max}$ and predicted most probable forces with experimental results for cyclopropanes (CP), benzocyclobutenes (BCB) and diarylethenes (DAE)

Fig. S9 depicts the $F_{\max}$ and calculated most probable force values in comparison with the experimentally measured values. As can be seen, the predicted values agree more quantitatively to the measured values than $F_{\max}$.

S6 Detailed reactions

We list all reactions measured and calculated in detail below in Table S3. The parameters and values from experimental work are listed at first, followed by the calculated spring constant from force extension curve. If this value is higher than the cantilever spring constant, the loading rate value is calculated using the latter value.

Following this, we see the COGEF initial and final structures obtained using DFT with PBE functional. The force variation against the breaking bond is plotted and the maximum corresponds to the force for ring opening reaction without considering temperature effects. Using NEB method, the force independent barrier calculation with COGEF initial and final states is also considered. For rule violation cases, additional NEB barrier for WH/WHD-allowed altered reaction is considered. The structure and stick diagrams for the same are listed.

The corrected barrier is lower in energy and therefore is the correct dissociation energy in the absence of force. We use this barrier value for most probable force calculations which is also listed.

Table S3: Reactions of individual molecules with given and calculated parameters

CP1. Syn-Cl gCFC	
Experimental parameters from [19]	
k_c (nN/Å)	0.002
v_c (Å/s)	3000
SMFS measured force (nN)	1.5 ± 0.07
Calculated parameters	
k_{total} (nN/Å)	0.0036 (higher than k_c)
α_{calc} (nN/s)	6

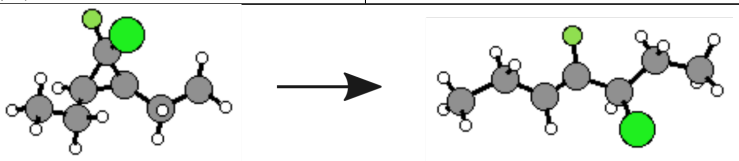

COGEF: Disrotatory outward

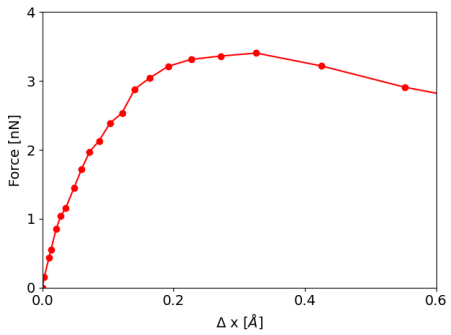

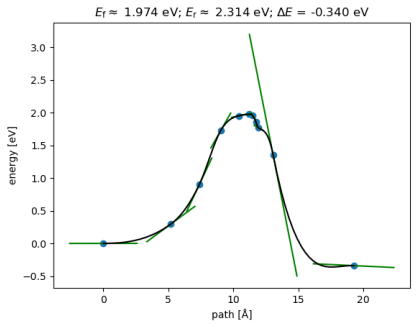

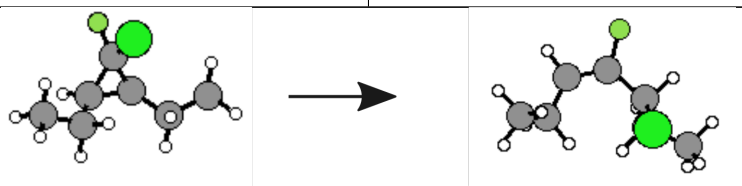

WHD rule: Disrotatory inward

Table S3: (continued)

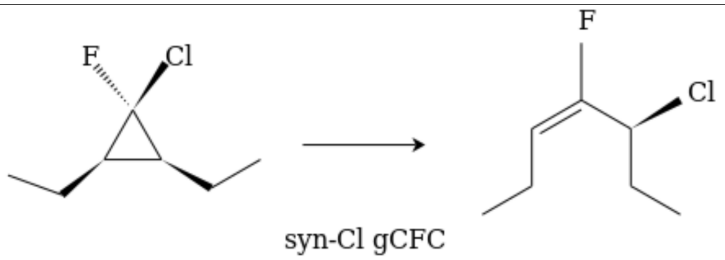

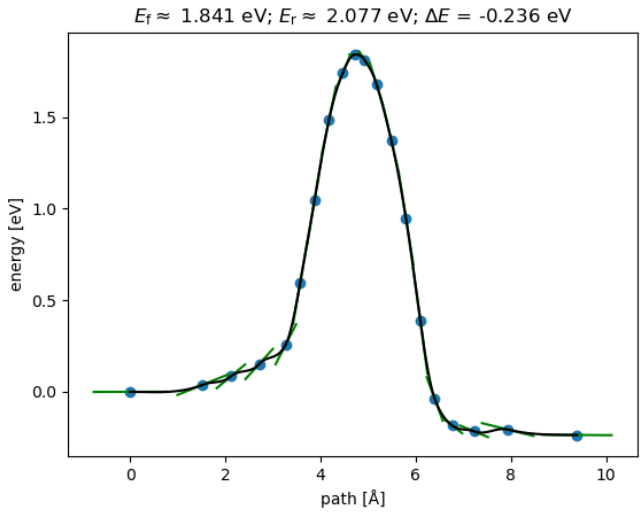

COGEF $F_{\max}$ (nN)	3.4, 3.5 [32]
NEB barrier (eV)	1.84
Most probable force (nN)	1.41 ± 0.05
CP2. Anti-Cl gCFC	
Experimental parameters from [19]	
k_c (nN/Å)	0.002
v_c (Å/s)	3000
SMFS measured force (nN)	1.29 ± 0.07
Calculated parameters	
k_{total} (nN/Å)	0.00075
α_{calc} (nN/s)	2.27

Table S3: (continued)

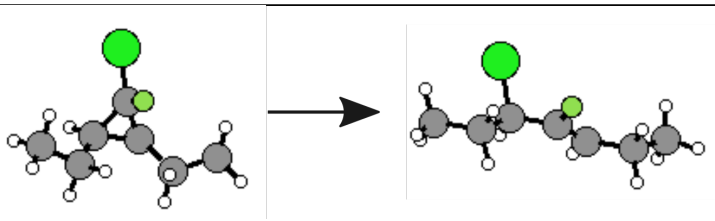

COGEF and WHD rule: Disrotatory outward

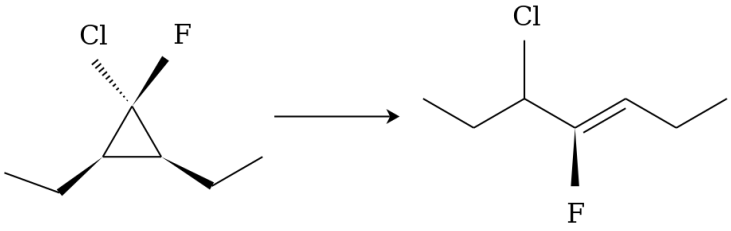

anti-Cl gCFC

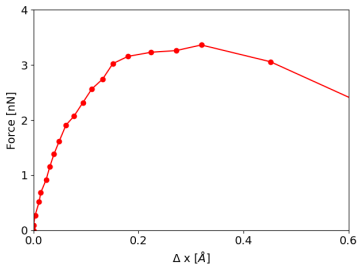

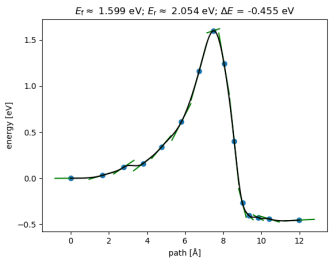

COGEF $F_{\max}$ (nN)	3.36, 3.2 [32]
NEB barrier (eV)	1.6
Most probable force (nN)	1.2 ± 0.05

CP3. gDBC PNB	
Experimental parameters from [20]	
k_c (nN/Å)	0.002
v_c (Å/s)	30000
α (nN/s)	2-5 (3.5)
SMFS measured force (nN)	0.74 ± 0.08
Calculated parameters	

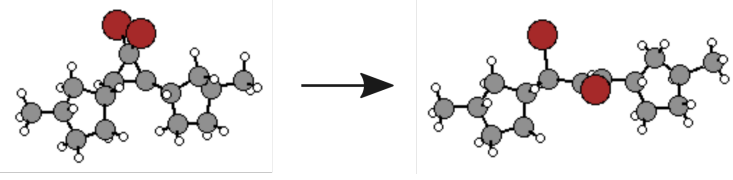

Table S3: (continued)

COGEF and WHD rule: Disrotatory outward	
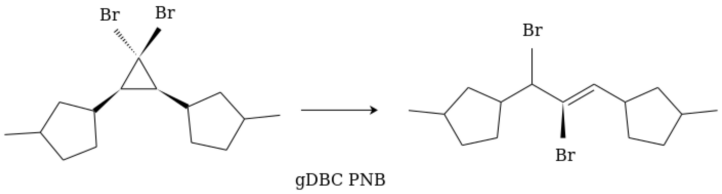	
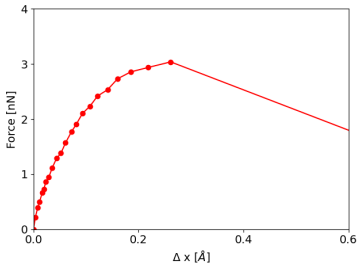	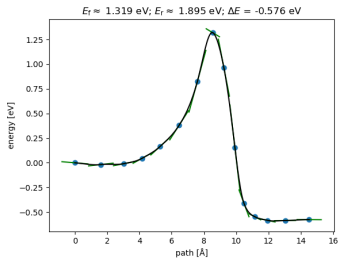
COGEF $F_{\max}$ (nN)	3.04, 3.3 [32]
NEB barrier (eV)	1.32
Most probable force (nN)	0.91 ± 0.05
CP4. gDBC PB	
Experimental parameters from [20]	
k_c (nN/Å)	0.002
v_c (Å/s)	30000
α (nN/s)	2-5 (3.5)
SMFS measured force (nN)	1.21 ± 0.1
Calculated parameters	
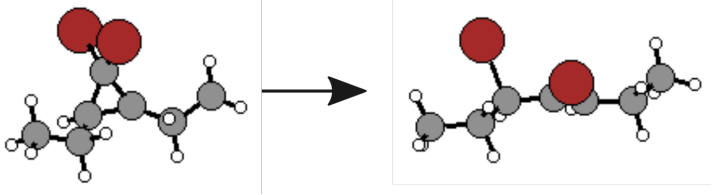	
COGEF and WHD rule: Disrotatory outward	

Table S3: (continued)

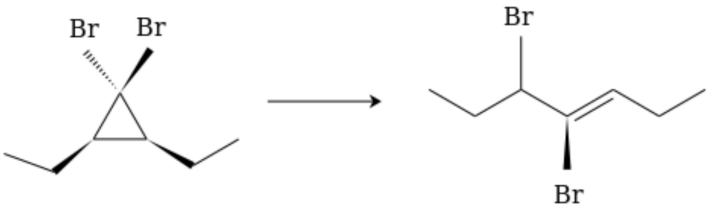

gDBC PB

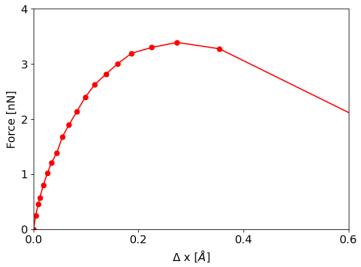

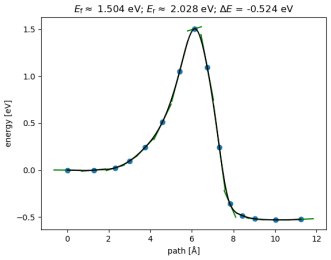

COGEF $F_{\max}$ (nN)	3.39, 3.7 [32]
NEB barrier (eV)	1.5
Most probable force (nN)	1.16 ± 0.05

CP5. gDCC PB/cis gDCC

Experimental parameters from [20]

k_c (nN/Å)	0.002
v_c (Å/s)	30000
α (nN/s)	2-5 (3.5)
SMFS measured force (nN)	1.33 ± 0.07

Calculated parameters

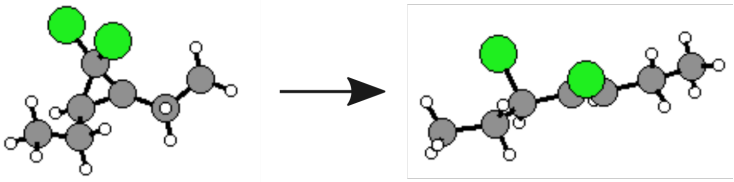

COGEF and WHD rule: Disrotatory outward

Table S3: (continued)

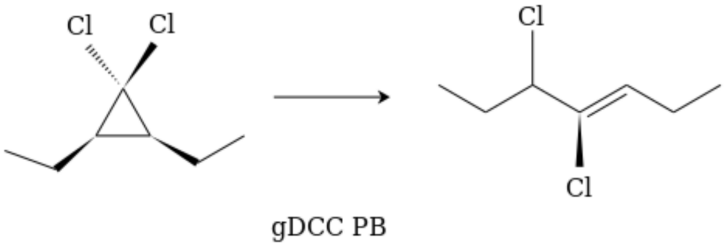

gDCC PB

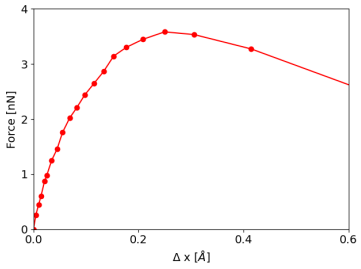

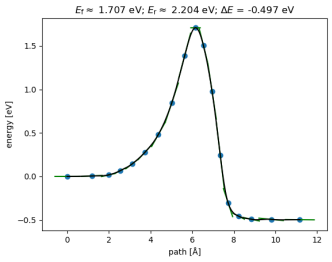

COGEF $F_{\max}$ (nN)	3.58, 3.8 [32]
NEB barrier (eV)	1.7
Most probable force (nN)	1.37 ± 0.05

CP6. Trans gDCC	
Experimental parameters from [22]	
k_c (nN/Å)	0.002
v_c (Å/s)	3000
SMFS measured force (nN)	2.3 ± 0.1
Calculated parameters	
k_{total} (nN/Å)	0.0041 (higher than k_c)
α_{calc} (nN/s)	6

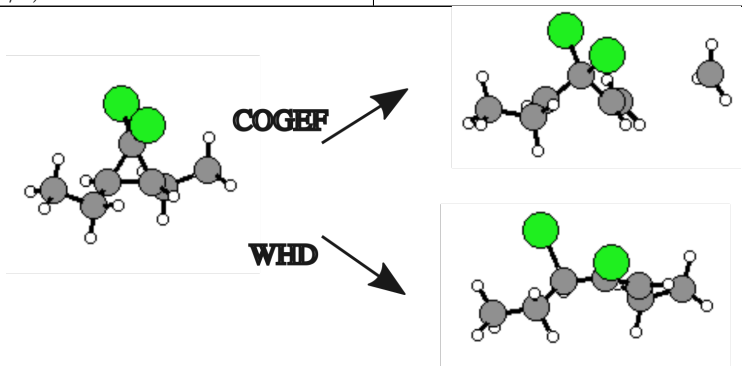

COGEF: no migration, WHD rule: Disrotatory outward

Table S3: (continued)

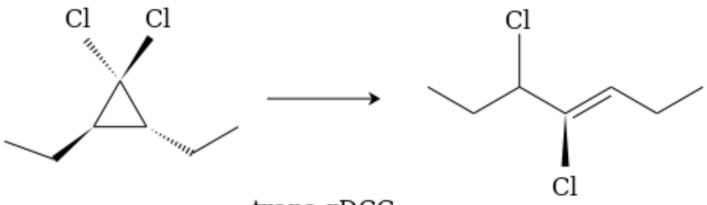

trans gDCC

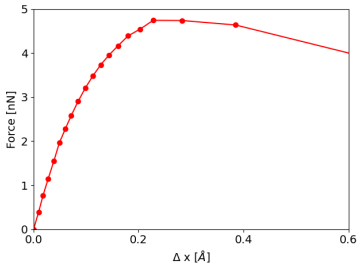

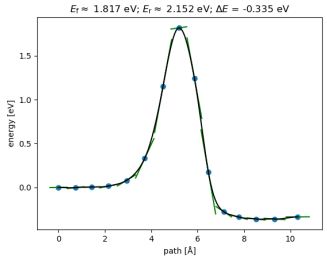

COGEF $F_{\max}$ (nN)	4.74, 5.2 [32]
NEB barrier (eV)	1.82
Most probable force (nN)	1.92 ± 0.07

CP7. gDCC PNB

Experimental parameters from [20]

k_c (nN/Å)	0.002
v_c (Å/s)	30000
α (nN/s)	2-5 (3.5)
SMFS measured force (nN)	0.9 ± 0.04

Calculated parameters

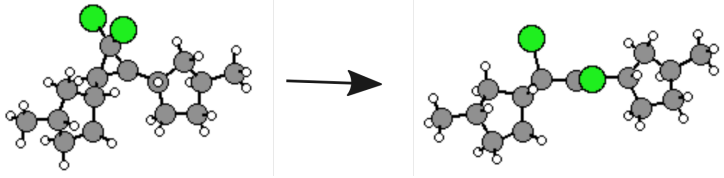

COGEF and WHD rule: Disrotatory outward

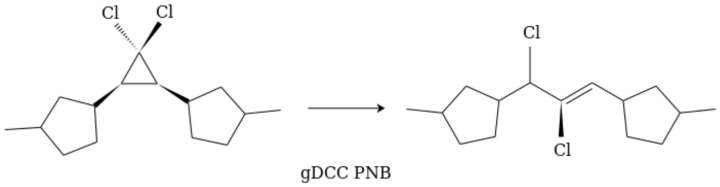

gDCC PNB

Table S3: (continued)

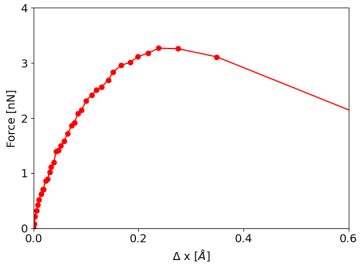	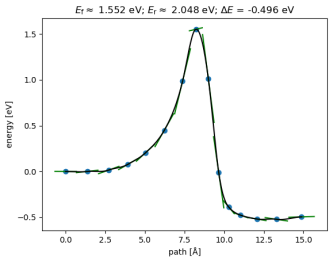
COGEF $F_{\max}$ (nN)	3.27, 3.4 [32]
NEB barrier (eV)	1.55
Most probable force (nN)	1.16 ± 0.05
CP8. E-α-alkene-gDCC	
Experimental parameters from [24]	
k_c (nN/Å)	0.002
v_c (Å/s)	3000
SMFS measured force (nN)	0.8 ± 0.04
Calculated parameters	
k_{total} (nN/Å)	0.0012
α_{calc} (nN/s)	3.71
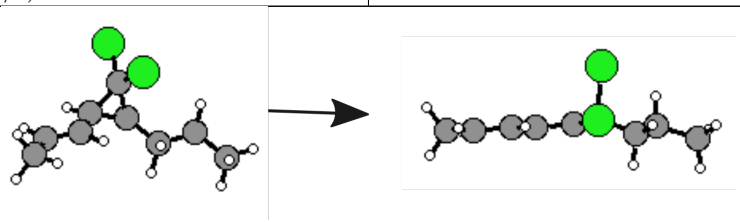 COGEF and WHD rule: Disrotatory outward	
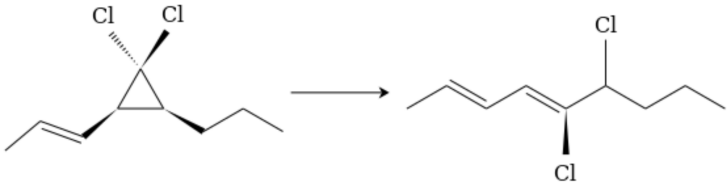 E-α-alkene-gDCC	

Table S3: (continued)

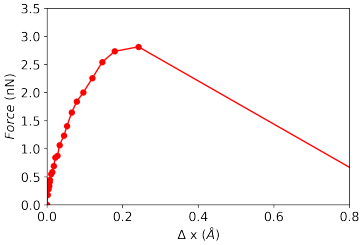	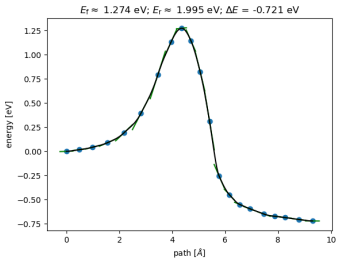
COGEF $F_{\max}$ (nN)	2.81, 3.2 [32]
NEB barrier (eV)	1.27
Most probable force (nN)	0.81 ± 0.05
CP9. Z-α-alkene-gDCC	
Experimental parameters from [24]	
k_c (nN/Å)	0.002
v_c (Å/s)	3000
SMFS measured force (nN)	1.16 ± 0.05
Calculated parameters	
k_{total} (nN/Å)	0.0017
α_{calc} (nN/s)	5.07
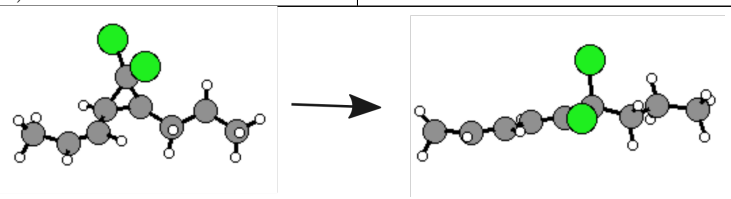 COGEF and WHD rule: Disrotatory outward	
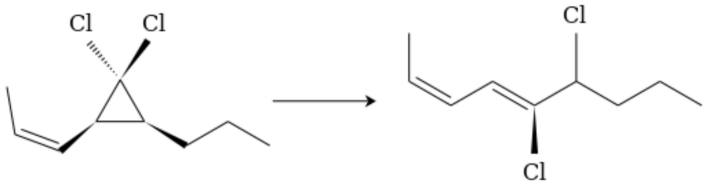 Z-α-alkene-gDCC	

Table S3: (continued)

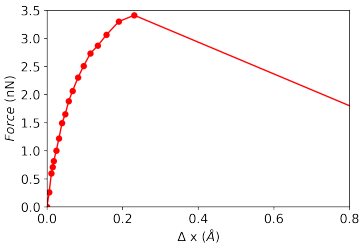	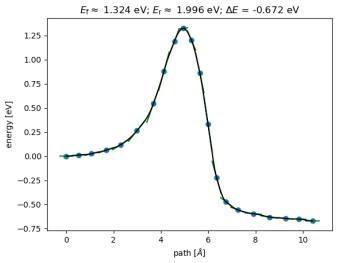
COGEF $F_{\max}$ (nN)	3.41, 3.7[32]
NEB barrier (eV)	1.32
Most probable force (nN)	1.03 ± 0.06
BCB1. Trans BCB	
Experimental parameters from [22]	
k_c (nN/Å)	0.002
v_c (Å/s)	3000
SMFS measured force (nN)	1.5 ± 0.06
Calculated parameters	
k_{total} (nN/Å)	0.0042 (higher than k_c)
α_{calc} (nN/s)	6
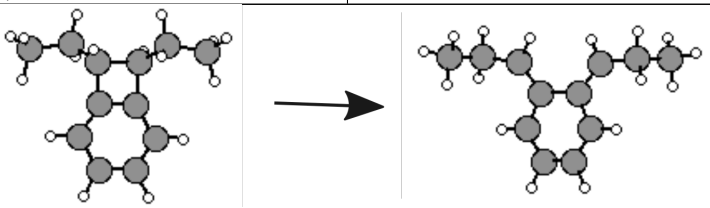 COGEF and WH rule: Conrotatory	
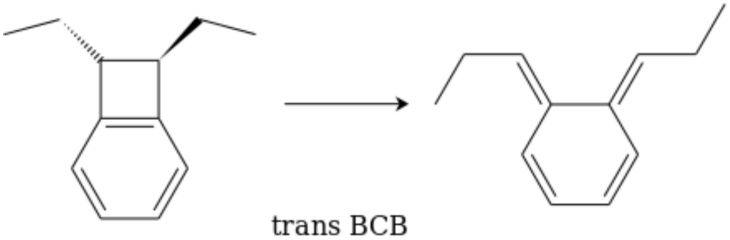	

Table S3: (continued)

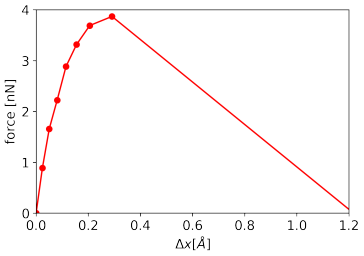	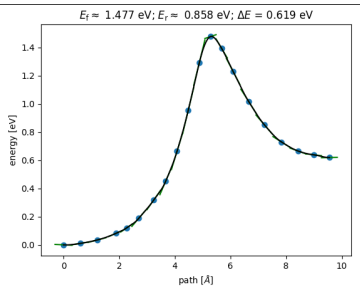
COGEF $F_{\max}$ (nN)	3.87, 4.1[32]
NEB barrier (eV)	1.48
Most probable force (nN)	1.33 ± 0.06
BCB2. Cis BCB	
Experimental parameters from [22]	
k_c (nN/Å)	0.002
v_c (Å/s)	3000
SMFS measured force (nN)	1.37 ± 0.08
Calculated parameters	
k_{total} (nN/Å)	0.0039 (higher than k_c)
α_{calc} (nN/s)	6
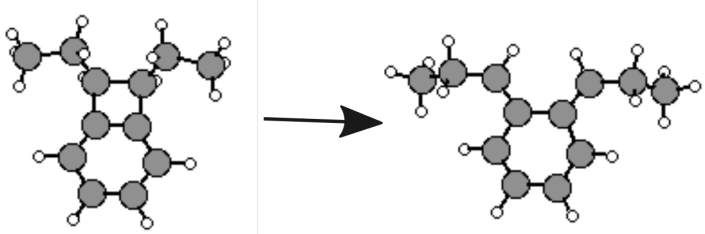	
COGEF: Disrotatory	
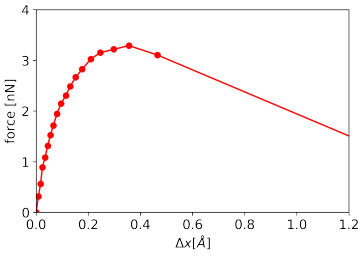	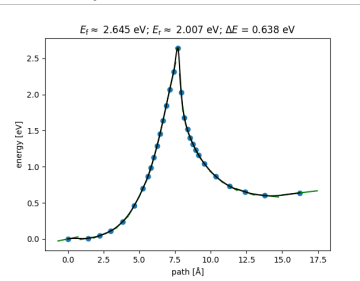

Table S3: (continued)

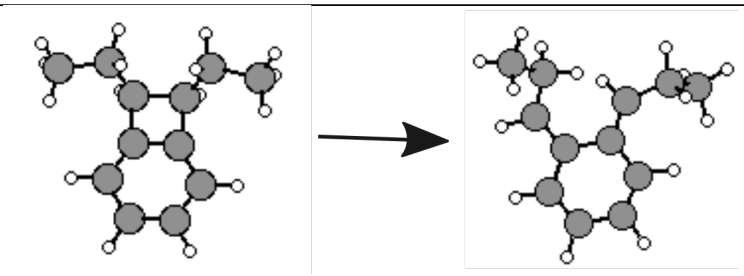

WH rule: Conrotatory

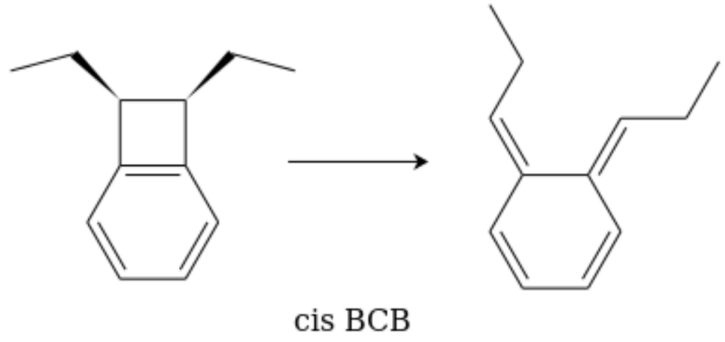

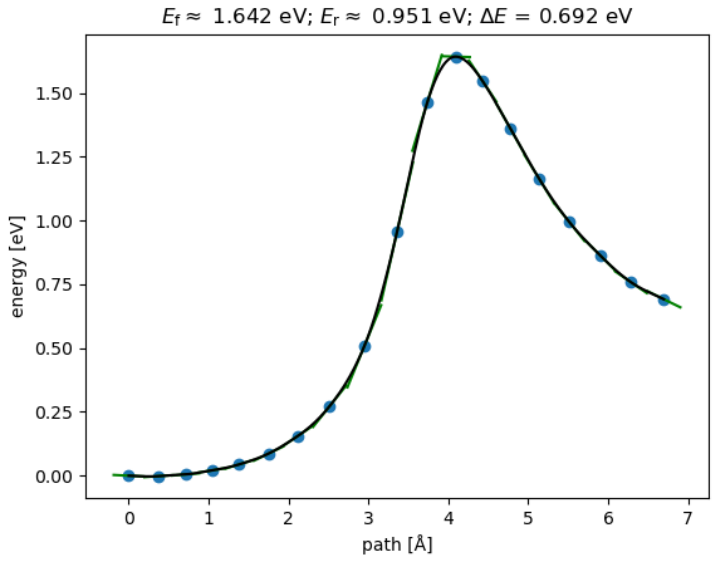

COGEF F_{max} (nN)	3.4, 3.7[32]
NEB barrier (eV)	1.64
Most probable force (nN)	1.28 ± 0.05

Table S3: (continued)

BCB3. Z-α-alkene-BCB	
Experimental parameters from [25]	
v_c (Å/s)	3000
SMFS measured force (nN)	1.25
Calculated parameters	
k_{total} (nN/Å)	0.0016
α_{calc} (nN/s)	4.7
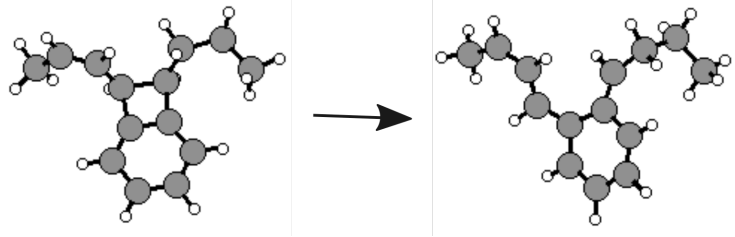 COGEF and WH rule: Conrotatory	
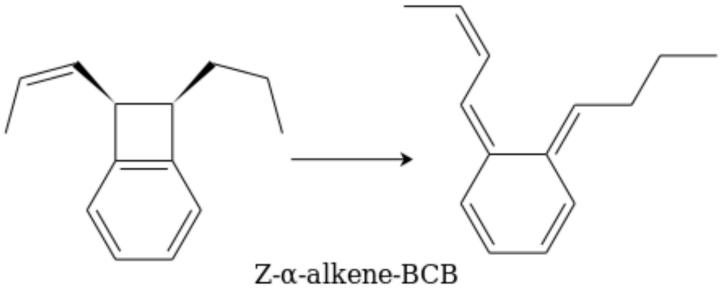	
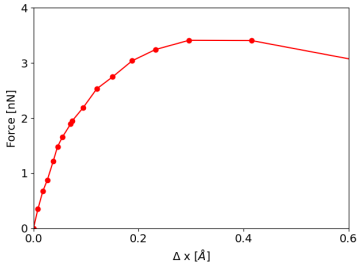	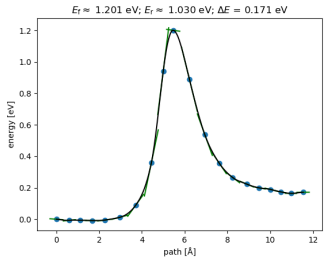
COGEF $F_{\max}$ (nN)	3.45, 3.7[32]
NEB barrier (eV)	1.2
Most probable force (nN)	0.91 ± 0.06
BCB4. E-α-alkene-BCB	
Experimental parameters from [25]	
v_c (Å/s)	3000
SMFS measured force (nN)	0.92 ± 0.06

Table S3: (continued)

Calculated parameters	
k_{total} (nN/Å)	0.0016
α_{calc} (nN/s)	4.7

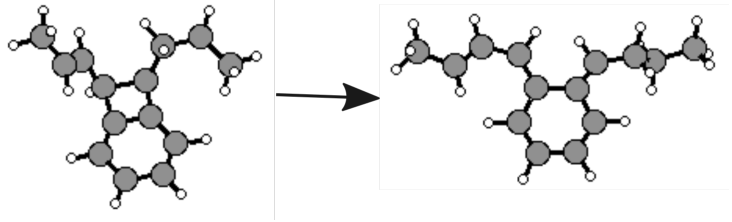

COGEF: Disrotatory

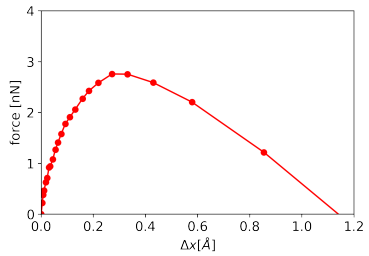

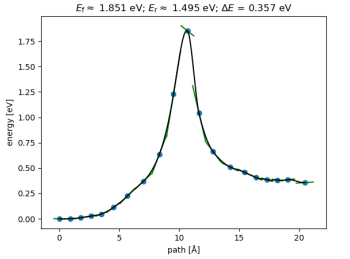

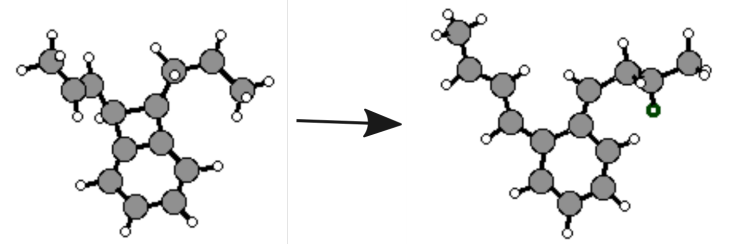

WH rule: Conrotatory

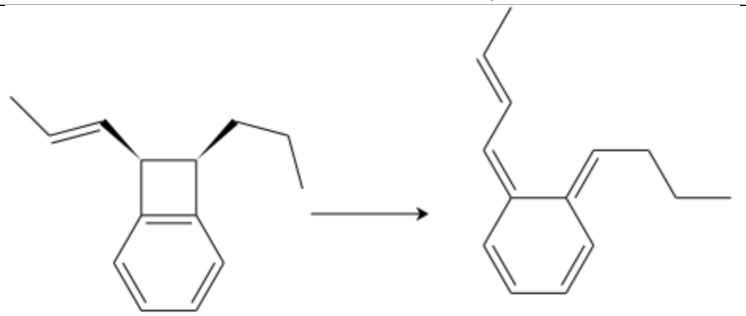

E-α-alkene-BCB

Table S3: (continued)

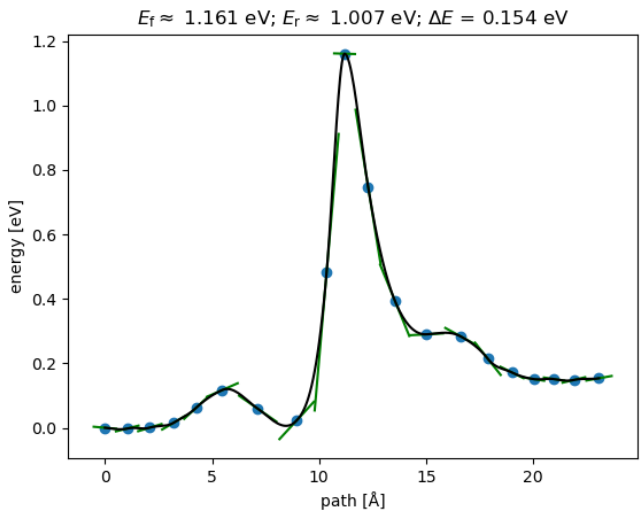

COGEF $F_{\max}$ (nN)	2.86, 3.1[32]
NEB barrier (eV)	1.16
Most probable force (nN)	0.68 ± 0.05

Symbols used:
k_c : cantilever spring constant
v_c : retraction velocity of the cantilever
k_{total} : total spring constant of cantilever and the considered molecules, from force extension curve
α_{calc} : loading rate calculated from curve = $k_{total}\ v_c$
α_{calc} : = $k_c\ v_c$, if $k_c < k_{total}$
Some papers have derived the loading rates from force curves which are listed as α in the experimental parameters.

References

[1] F. Hanke, H. J. Kreuzer. *Physical Review E - Statistical, Nonlinear, and Soft Matter Physics* **2006**, *74*, 1–5.

[2] S. Khodayeki, W. Maftuhin, M. Walter. *ChemPhysChem* **2022**, *n/a*, e202200237.

[3] G. I. Bell. *Science* **1978**, *200*, 618–627.

[4] E. Evans, K. Ritchie. *Biophysical Journal* **1997**, *72*, 1541–1555.

[5] E. Evans, K. Ritchie. *Biophysical Journal* **1999**, *76*, 2439–2447.

[6] A. Garg. *Physical Review B* **1995**, *51*, 15592–15595.

[7] O. K. Dudko, G. Hummer, A. Szabo. *Physical Review Letters* **2006**, *96*, 108101.

[8] O. K. Dudko, J. Mathé, A. Szabo, A. Meller, G. Hummer. *Biophysical Journal* **2007**, *92*, 4188–4195.

[9] R. W. Friddle, A. Noy, J. J. De Yoreo. *Proc. Natl. Acad. Sci. U.S.A.* **2012**, *109*, 13573–13578.

[10] R. W. Friddle. *Phys. Rev. Lett.* **2008**, *100*, 138302.

[11] J. T. Bullerjahn, S. Sturm, K. Kroy. *Nature Communications* **2014**, *5*, 4463.

[12] A. Maitra, G. Arya. *Phys. Rev. Lett.* **2010**, *104*, 108301.

[13] G. Hummer, A. Szabo. *Biophysical Journal* **2003**, *85*, 1–11.

[14] Z. Li, I. Szlufarska. *Physical Review Letters* **2021**, *126*, 76001.

[15] S. Akbulatov, Y. Tian, R. Boulatov. *Journal of the American Chemical Society* **2012**, *134*, 7620–7623.

[16] M. Wollenhaupt, C. Schran, M. Krupička, D. Marx. *ChemPhysChem* **2018**, *19*, 837–847.

[17] G. Henkelman, H. Jónsson. *Journal of Chemical Physics* **2000**, *113*, 9978–9985.

[18] O. Brügner, M. Walter. *Physical Review Materials* **2018**, *2*, 1–6.

[19] J. Wang, T. B. Kouznetsova, S. L. Craig. *J. Am. Chem. Soc.* **2014**, *137*, 11554–11557.

[20] H. M. Klukovich, T. B. Kouznetsova, Z. S. Kean, J. M. Lenhardt, S. L. Craig. *Nature Chemistry* **2013**, *5*, 110–114.

[21] O. N. Faza, C. S. López, R. Álvarez, A. R. de Lera. *J. Org. Chem.* **2004**, *69*, 9002–9010.

[22] J. Wang, T. B. Kouznetsova, Z. Niu, M. T. Ong, H. M. Klukovich, A. L. Rheingold, T. J. Martinez, S. L. Craig. *Nature Chemistry* **2015**, *7*, 323–327.

[23] W. E. Parham, K. S. Yong. *J. Org. Chem.* **1968**, *33*, 3947–3948.

[24] J. Wang, T. B. Kouznetsova, Z. S. Kean, L. Fan, B. D. Mar, T. J. Martínez, S. L. Craig. *Journal of the American Chemical Society* **2014**, *136*, 15162–15165.

[25] J. Wang, T. B. Kouznetsova, Z. Niu, A. L. Rheingold, S. L. Craig. *Journal of Organic Chemistry* **2015**, *80*, 11895–11898.

[26] J. Wang, T. B. Kouznetsova, Z. S. Kean, L. Fan, B. D. Mar, T. J. Martínez, S. L. Craig. *Journal of the American Chemical Society* **2014**, *136*, 15162–15165.

[27] R. B. Woodward, R. Hoffmann. *J. Am. Chem. Soc.* **1965**, *87*, 395–397.

[28] R. B. Woodward, R. Hoffmann. *Angew. Chem. Int. Ed. Engl.* **1969**, *8*, 781–853.

[29] C. H. DePuy. *Acc. Chem. Res.* **1968**, 33–41.

[30] M. T. Ong, J. Leiding, H. Tao, A. M. Virshup, T. J. Martínez. *J. Am. Chem. Soc.* **2009**, *131*, 6377–6379.

[31] M. Wollenhaupt, M. Krupička, D. Marx. *ChemPhysChem* **2015**, *16*, 1593–1597.

[32] I. M. Klein, C. C. Husic, D. P. Kovács, N. J. Choquette, M. J. Robb. *Journal of the American Chemical Society* **2020**, *142*, 16364–16381.

[33] P. J. Stephens, F. J. Devlin, C. F. Chabalowski, M. J. Frisch. *J. Phys. Chem.* **1994**, *98*, 11623–11627.

[34] J. P. Perdew, K. Burke, M. Ernzerhof. *Physical Review Letters* **1996**, *77*, 3865–3868.

[35] M. F. Iozzi, T. Helgaker, E. Uggerud. *Molecular Physics* **2009**, *107*, 2537–2546.

[36] C. Zhang, T. B. Kouznetsova, B. Zhu, L. Sweeney, M. Lancer, I. Gitsov, S. L. Craig, X. Hu. *Journal of the American Chemical Society* **2025**, *147*, 2502–2509.